JOURNAL OF APPLIED PHYSICS **113**, 123506 (2013)

Phase-field modeling of martensitic microstructure with inhomogeneous elasticity

H. Z. Chen and Y. C. Shu[a)]
Institute of Applied Mechanics, National Taiwan University, Taipei 106, Taiwan

(Received 22 February 2013; accepted 6 March 2013; published online 28 March 2013)

A phase-field model accounting for elastic inhomogeneity is established for microstructure study in martensitic materials. It is motivated by Hashin-Shtrikman variational formulation by introducing a homogeneous comparison medium and a polarized stress field. As a result, the driving force due to stress can be computed in the equivalent homogeneous medium since it is formally identical to that in the actual inhomogeneous solid. The model is applied to the simulations of three-dimensional self-accommodation patterns of microstructure for tetragonal and trigonal martensite. The results show that the former is an atypical pattern while the latter exhibits a common herringbone structure. Finally, the proposed framework also offers advantages of modeling other phase-transforming materials with ability in domain simulations together with effective properties as byproduct. © *2013 American Institute of Physics*. [http://dx.doi.org/10.1063/1.4796098]

I. INTRODUCTION

Martensitic microstructure is the result of a solid-to-solid phase transformation during which there is a sudden change in the crystal structure at a certain temperature.[1–3] It exhibits relative shape change between crystal lattices of the high and low temperature phases. Besides, such a switch is of an orientation dependence due to symmetry breaking, giving rise to numerous orientation-related variants below transition temperature. A key feature of martensitic microstructure is the observations of various intriguing and fascinating fine-scale patterns formed by variants. The manipulation of patterns of microstructure provides a novel strategy in many applications. For example, recent studies have shown that certain characteristic distortion of martensitic patterns can be utilized as components of tiny machines.[4] Another important application of martensitic transformation is the shape recovery on heating observed in certain alloys.[5–8]

The arrangements of these variants are, however, not arbitrary. They have to keep the interfaces coherent for avoiding generations of dislocations and voids. Thus, strain compatibility plays a central role in pattern formation of variants. This issue has been studied theoretically based on the crystallographic theory of martensite in an early stage[9,10] and on the energy minimization of nonconvex functionals subsequently.[11–13] While these theoretical achievements provide understanding on why and how variants form non-generic microstructure patterns, obtaining patterns within a general framework is not an easy task. This motivates many more research efforts being focus on developing models based on atomic descriptions to continuum frameworks for numerical simulations.[14–18] Among them, phase-field models are particularly popular due to no prior assumptions on the profiles and tracking of interfaces.[19–23] Advances in computer simulations include results from single crystals,[24,25] multilayers,[26,27] and polycrystals.[28,29] Alternative formulation based on the equations of strain compatibility have also been proposed for pattern simulation.[30–32]

In spite of many fruitful results from the phase-field simulations of martensite, there is one drawback that the elastic modulus differences of distinct phases are often neglected.[33] Indeed, conventional phase-field approaches choose the transformation strains of variants as order parameters and expand them in terms of polynomials at high orders in the energy formulation. As a result, the elastic moduli remain unchanged for different martensitic phases, leading to an elastically homogeneous while structurally inhomogeneous formulation. To allow varying elastic moduli for each martensitic variant, an unconventional phase-field model is adopted here for pattern simulation. This approach chooses the characteristic functions of transforming variants as the field variables, showing advantages of expressing energy-well structure explicitly and maintaining material symmetry.[34–37] To overcome the difficulty in solving mechanical equilibrium with elastic inhomogeneity, an idea based on Eshelby's equivalent inclusion principle is adopted.[38] It involves the introduction of a fictitious eigenstrain in a comparison homogeneous medium so that strain and stress fields in this equivalent medium are identical to those in the original inhomogeneous solid. This approach combined with Khachaturyan's microelasticity theory has been first proposed by Wang *et al.*[39] and subsequently by other researchers in different problems.[40–43] Recently, improvements have been proposed by Shen *et al.*[44] for implementing damped iterative algorithm and by Wang *et al.*[45] for incorporating Fourier spectral iterative-perturbation algorithm.[46,47] Another method based on the fast iterative algorithm for computing inhomogeneous elasticity has been proposed by Moulinec and Suquet[48–50] and by their coworkers for improvement.[51–53]

Different from the framework proposed by Wang *et al.*[39] for elastically and structurally inhomogeneous systems, this article proposes an alternative energy formulation based on the spirit of Hashin-Shtrikman variational principle.[54,55] The

[a)]Author to whom correspondence should be addressed. Electronic mail: yichung@iam.ntu.edu.tw

formulation is subsequently implemented to the unconventional phase-field model for microstructure simulation accounting for elastic inhomogeneity of different phases. Indeed, let $\mathbf{C}^{(i)}$ and $\mathbf{C}^{(j)}$ be the elastic tensor of the ith and jth martensitic variants. They are related by the tensorial transformation with respect to certain rotation transforming the ith variant to the jth variant. Thus, a strong elastic inhomogeneity is expected in the solids of martensite, leading to an interest in determining effective material properties. Such an issue is particularly important in certain class of phase-transforming materials. For example, the dramatically enhanced piezoelectricity in relaxor ferroelectric single crystals has been explained by the effective electromechanical moduli of engineered domain configurations.[56,57] Thus, the proposed framework serves as a useful tool for microstructure simulation with effective properties as byproduct. Besides, the extension to the polarizable model of ferroelectrics accounting for inhomogeneity of electromechanical moduli has been carried out and will be presented elsewhere.[58]

II. MODELING

A. Transformation strain

A single crystal of austenite transforms to a martensite as it is cooled. Typically, the austenite phase has cubic symmetry while the martensite phase has smaller symmetry such as tetragonal, trigonal, orthorhombic, or monoclinic symmetry. This gives rise to N symmetry-related variants of martensite.[59] If the reference configuration is chosen as that occupied by an austenite at the critical temperature, the transformation from the austenite to the ith variant of martensite is described by the transformation strains $\boldsymbol{\epsilon}^{(i)}$. They are determined from the change of symmetry and lattice parameters. For example, consider a tetragonal martensite. There are three martensitic variants with transformation strains

$$\boldsymbol{\epsilon}_{tet}^{(1)} = \begin{pmatrix} \eta_2 & 0 & 0 \\ 0 & \eta_1 & 0 \\ 0 & 0 & \eta_1 \end{pmatrix}, \quad \boldsymbol{\epsilon}_{tet}^{(2)} = \begin{pmatrix} \eta_1 & 0 & 0 \\ 0 & \eta_2 & 0 \\ 0 & 0 & \eta_1 \end{pmatrix}, \quad \boldsymbol{\epsilon}_{tet}^{(3)} = \begin{pmatrix} \eta_1 & 0 & 0 \\ 0 & \eta_1 & 0 \\ 0 & 0 & \eta_2 \end{pmatrix}. \tag{1}$$

Above η_1 and η_2 are material parameters which are determined by measuring changes in crystal bases of different phases.[60] The schematic view of these three variants is depicted in the left part of Fig. 1 where a cubic lattice is stretched along one of the crystal basis directions. Another common case is the trigonal martensite which has four variants described by

$$\boldsymbol{\epsilon}_{trig}^{(1)} = \begin{pmatrix} \alpha & \delta & \delta \\ \delta & \alpha & \delta \\ \delta & \delta & \alpha \end{pmatrix}, \quad \boldsymbol{\epsilon}_{trig}^{(2)} = \begin{pmatrix} \alpha & -\delta & -\delta \\ -\delta & \alpha & \delta \\ -\delta & \delta & \alpha \end{pmatrix}, \quad \boldsymbol{\epsilon}_{trig}^{(3)} = \begin{pmatrix} \alpha & \delta & -\delta \\ \delta & \alpha & -\delta \\ -\delta & -\delta & \alpha \end{pmatrix}, \quad \boldsymbol{\epsilon}_{trig}^{(4)} = \begin{pmatrix} \alpha & -\delta & \delta \\ -\delta & \alpha & -\delta \\ \delta & -\delta & \alpha \end{pmatrix}, \tag{2}$$

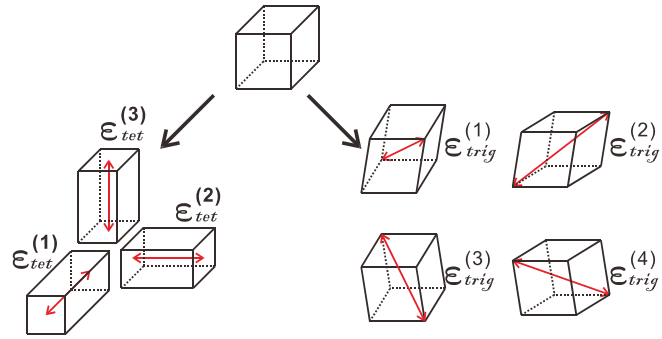

FIG. 1. Schematic of diffusionless solid to solid martensitic phase transformation. The left part shows cubic-to-tetragonal transformation, while the right side shows cubic-to-trigonal transformation. The arrows indicate the direction of distortion of a cube.

and α and δ are material parameters.[3] The schematic view of these 4 variants is depicted in the right part of Fig. 1 where distortion is obtained by stretching the cubic lattice along one of body diagonal directions. The expression of transformation strains for other cases such as orthorhombic and monoclinic martensitic crystals can be found in Ref. 59.

Let Ω be the region occupied by the crystal and Ω_i be the subregion occupied by the ith martensitic variant for $i = 1, 2, \ldots, N$ at the low temperature. Thus, $\Omega_i \cap \Omega_j = \varnothing$ if $i \neq j$. Let $\boldsymbol{\epsilon}^*(\mathbf{x})$ represent the locally inhomogeneous transformation strain field such that $\boldsymbol{\epsilon}^*(\mathbf{x}) = \boldsymbol{\epsilon}^{(i)}$ if $\mathbf{x} \in \Omega_i$; or equivalently,

$$\boldsymbol{\epsilon}^*(\mathbf{x}) = \sum_{i=1}^{N} \lambda_i(\mathbf{x}) \boldsymbol{\epsilon}^{(i)}, \tag{3}$$

where $\lambda_i(\mathbf{x})$ is the space characteristic function such that $\lambda_i(\mathbf{x}) = 1$ if $\mathbf{x} \in \Omega_i$ and $\lambda_i(\mathbf{x}) = 0$ otherwise. Physically, the volume average of λ_i stands for the volume fraction of the ith martensitic variant.

B. Elastic strain energy

The elastic strain energy of a martensite is described by

$$\mathcal{I}^{elas} = \int W^{elas} d\mathbf{x} = \int \frac{1}{2} (\boldsymbol{\epsilon} - \boldsymbol{\epsilon}^*) \cdot \mathbf{C}(\mathbf{x}) (\boldsymbol{\epsilon} - \boldsymbol{\epsilon}^*) d\mathbf{x}, \tag{4}$$

where $\boldsymbol{\epsilon}$ is the compatible strain related to displacement $\mathbf{u}$ by $\boldsymbol{\epsilon} = \frac{1}{2}[\nabla \mathbf{u} + (\nabla \mathbf{u})^T]$. Above $\mathbf{C}$ is the elastic 4-tensor and is positive-definite symmetric such that C_{ijkl}, the components of $\mathbf{C}$ in some orthonormal basis, follow

$$C_{ijkl} = C_{ijlk} = C_{klij}, \quad i, j, k, l = 1, 2, 3. \tag{5}$$

The stress inside the material is

$$\boldsymbol{\sigma}(\mathbf{x}) = \mathbf{C}(\mathbf{x})(\boldsymbol{\epsilon} - \boldsymbol{\epsilon}^*). \tag{6}$$

As the elastic modulus $\mathbf{C}$ varies from phases to phases, it is no longer a constant and depends on positions, giving rise to difficulty in computing stress fields. To resolve this problem, consider an alternative form of elastic strain energy motivated from the famous Hashin-Shtrikman formulation[54,55]

$$\mathcal{I}_{HS}^{elas} = \int W_{HS}^{elas} d\mathbf{x} = \int \left\{ \frac{1}{2}(\mathbf{p} - \mathbf{C}^0\boldsymbol{\epsilon}^*) \cdot (\mathbf{C}^0 - \mathbf{C})^{-1}(\mathbf{p} - \mathbf{C}^0\boldsymbol{\epsilon}^*) - \frac{1}{2}\mathbf{p} \cdot \boldsymbol{\Gamma}\mathbf{p} - \langle\boldsymbol{\epsilon}\rangle \cdot \mathbf{p} + \boldsymbol{\epsilon}^* \cdot \mathbf{p} - \frac{1}{2}\boldsymbol{\epsilon}^* \cdot \mathbf{C}^0\boldsymbol{\epsilon}^* \right\} d\mathbf{x}. \quad (7)$$

Above $\mathbf{C}^0$ is the elastic modulus of a homogeneous comparison material, $\mathbf{p}$ is a polarized stress field, $\langle\epsilon\rangle$ is the average of strain, and $\boldsymbol{\Gamma}$ is the linear operator producing from polarized stress $\mathbf{p}$ a strain with zero average. In other words,

$$\boldsymbol{\epsilon}' = \boldsymbol{\Gamma}\mathbf{p}, \quad \langle\boldsymbol{\epsilon}'\rangle = \mathbf{0}. \quad (8)$$

The explicit operation of $\boldsymbol{\Gamma}$ in the Fourier transform space can be found in the Appendix (see also Ref. 36). Note that the notion of polarized stress field $\mathbf{p}$ originally arising from the early work by Hashin and Shtrikman[54] can be related to the eigenstrain introduced by the Eshelby's equivalent inclusion method later.

To understand the above variational formulation, consider the first variation of Eq. (7) with respect to $\mathbf{p}$ and $\boldsymbol{\epsilon}^*$. This gives

$$\delta\mathcal{I}_{HS}^{elas} = -\int (\mathbf{F}_p^{elas} \cdot \delta\mathbf{p} + \mathbf{F}_{\varepsilon^*}^{elas} \cdot \delta\boldsymbol{\epsilon}^*) d\mathbf{x}, \quad (9)$$

where the driving forces $\mathbf{F}_p^{elas}$ and $\mathbf{F}_{\varepsilon^*}^{elas}$ are

$$\mathbf{F}_p^{elas} = -(\mathbf{C}^0 - \mathbf{C})^{-1}(\mathbf{p} - \mathbf{C}^0\boldsymbol{\epsilon}^*) + \boldsymbol{\Gamma}\mathbf{p} + \langle\boldsymbol{\epsilon}\rangle - \boldsymbol{\epsilon}^*, \quad (10)$$

$$\mathbf{F}_{\varepsilon^*}^{elas} = \mathbf{C}^0[(\mathbf{C}^0 - \mathbf{C})^{-1}(\mathbf{p} - \mathbf{C}^0\boldsymbol{\epsilon}^*)] - \mathbf{p} + \mathbf{C}^0\boldsymbol{\epsilon}^*. \quad (11)$$

Set the total strain $\boldsymbol{\epsilon}$ as

$$\boldsymbol{\epsilon} = \boldsymbol{\epsilon}' + \langle\boldsymbol{\epsilon}\rangle = \boldsymbol{\Gamma}\mathbf{p} + \langle\boldsymbol{\epsilon}\rangle. \quad (12)$$

The vanishing of the first variation with respect to $\delta\mathbf{p}$ in Eq. (10) gives

$$(\mathbf{C}^0 - \mathbf{C})^{-1}(\mathbf{p} - \mathbf{C}^0\boldsymbol{\epsilon}^*) = \boldsymbol{\epsilon} - \boldsymbol{\epsilon}^*.$$

In other words,

$$\mathbf{C}(\boldsymbol{\epsilon} - \boldsymbol{\epsilon}^*) = \mathbf{C}^0\boldsymbol{\epsilon} - \mathbf{p} = \mathbf{C}^0(\boldsymbol{\epsilon} - \boldsymbol{\epsilon}^0), \quad \mathbf{p} = \mathbf{C}^0\boldsymbol{\epsilon}^0. \quad (13)$$

This is exactly the conditions made by Eshelby's equivalent inclusion principle;[38] i.e., the strain and stress fields are identical in the original inhomogeneous material and an equivalent homogeneous solid. Such an equivalence is achieved by introducing a polarized stress field $\mathbf{p}$ or eigenstrain field $\boldsymbol{\epsilon}^0$ necessary for homogenization. In addition, the driving force $\mathbf{F}_{\varepsilon^*}^{elas}$ becomes

$$\mathbf{F}_{\varepsilon^*}^{elas} = \mathbf{C}^0(\boldsymbol{\epsilon} - \boldsymbol{\epsilon}^*) - \mathbf{C}^0\boldsymbol{\epsilon}^0 + \mathbf{C}^0\boldsymbol{\epsilon}^* = \mathbf{C}^0(\boldsymbol{\epsilon} - \boldsymbol{\epsilon}^0) = \boldsymbol{\sigma}. \quad (14)$$

Thus, $\mathbf{F}_{\varepsilon^*}^{elas}$ is interpreted as the stress field necessary for refining microstructure to accommodate the specified boundary constraints.[36]

Next, the relation between $\mathcal{I}^{elas}$ and $\mathcal{I}_{HS}^{elas}$ can be understood by evaluating their stationary values. Suppose the periodic boundary condition is enforced with average strain $\langle\boldsymbol{\epsilon}\rangle$ prescribed. For a fixed distribution of microstructure, the elastic energy $\mathcal{I}^{elas}$ in Eq. (4) at equilibrium is

$$\mathcal{I}^{elas} = \int \frac{1}{2}\boldsymbol{\sigma} \cdot \boldsymbol{\epsilon}' d\mathbf{x} + \int \frac{1}{2}\boldsymbol{\sigma} \cdot \langle\boldsymbol{\epsilon}\rangle d\mathbf{x} - \int \frac{1}{2}\boldsymbol{\sigma} \cdot \boldsymbol{\epsilon}^* d\mathbf{x} = \frac{1}{2}\int \langle\boldsymbol{\sigma}\rangle \cdot \langle\boldsymbol{\epsilon}\rangle d\mathbf{x} - \int \frac{1}{2}\boldsymbol{\sigma} \cdot \boldsymbol{\epsilon}^* d\mathbf{x}, \quad (15)$$

where the equilibrium condition $\nabla \cdot \boldsymbol{\sigma} = \mathbf{0}$ and periodic boundary condition are used in deriving the above formulation. Next, consider $\mathcal{I}_{HS}^{elas}$ in Eq. (7) at the stationary value. From Eq. (10) at the vanishing of $\mathbf{F}_p^{elas}$, Eq. (7) becomes

$$\mathcal{I}_{HS}^{elas} = \int \left\{ \frac{1}{2}(\mathbf{p} - \mathbf{C}^0\boldsymbol{\epsilon}^*) \cdot (\boldsymbol{\Gamma}\mathbf{p} + \langle\boldsymbol{\epsilon}\rangle - \boldsymbol{\epsilon}^*) - \frac{1}{2}\mathbf{p} \cdot \boldsymbol{\Gamma}\mathbf{p} - \langle\boldsymbol{\epsilon}\rangle \cdot \mathbf{p} + \boldsymbol{\epsilon}^* \cdot \mathbf{p} - \frac{1}{2}\boldsymbol{\epsilon}^* \cdot \mathbf{C}^0\boldsymbol{\epsilon}^* \right\} d\mathbf{x}$$
$$= -\int \frac{1}{2}\langle\boldsymbol{\epsilon}\rangle \cdot \mathbf{p} d\mathbf{x} - \int \frac{1}{2}\boldsymbol{\epsilon}^* \cdot [\mathbf{C}^0(\boldsymbol{\Gamma}\mathbf{p} + \langle\boldsymbol{\epsilon}\rangle) - \mathbf{p}] d\mathbf{x}$$
$$= \int \frac{1}{2}\langle\boldsymbol{\epsilon}\rangle \cdot \langle\boldsymbol{\sigma}\rangle d\mathbf{x} - \int \frac{1}{2}\boldsymbol{\sigma} \cdot \boldsymbol{\epsilon}^* d\mathbf{x} - \int \frac{1}{2}\langle\boldsymbol{\epsilon}\rangle \cdot \mathbf{C}^0\langle\boldsymbol{\epsilon}\rangle d\mathbf{x}, \quad (16)$$

where from Eq. (13) $\langle\mathbf{p}\rangle = -\langle\boldsymbol{\sigma}\rangle + \mathbf{C}^0\langle\boldsymbol{\epsilon}\rangle$. The comparison between Eqs. (15) and (16) provides

$$\mathcal{I}^{elas} = \mathcal{I}_{HS}^{elas} + \int \frac{1}{2}\langle\boldsymbol{\epsilon}\rangle \cdot \mathbf{C}^0\langle\boldsymbol{\epsilon}\rangle d\mathbf{x}. \quad (17)$$

In other words, the difference between $\mathcal{I}^{elas}$ and $\mathcal{I}_{HS}^{elas}$ per unit volume is a constant denoted by $\frac{1}{2}\langle\boldsymbol{\epsilon}\rangle \cdot \mathbf{C}^0\langle\boldsymbol{\epsilon}\rangle$.

Finally, the variational formulation in Eq. (7) is based on prescribing average strain $\langle\boldsymbol{\epsilon}\rangle$. Instead, if the overall stress $\langle\boldsymbol{\sigma}\rangle$ is provided, Eq. (7) is replaced as

$$\mathcal{I}_{HS*}^{elas} = \int W_{HS*}^{elas}(\boldsymbol{\epsilon}^0, \boldsymbol{\epsilon}^*) d\mathbf{x}, = \int \left\{ \frac{1}{2}(\boldsymbol{\epsilon}^0 - \boldsymbol{\epsilon}^*) \cdot (\mathbf{S} - \mathbf{S}^0)^{-1}(\boldsymbol{\epsilon}^0 - \boldsymbol{\epsilon}^*) - \frac{1}{2}\boldsymbol{\epsilon}^0 \cdot \boldsymbol{\Lambda}\boldsymbol{\epsilon}^0 - \langle\boldsymbol{\sigma}\rangle \cdot \boldsymbol{\epsilon}^0 \right\} d\mathbf{x}, \quad (18)$$

where $\mathbf{S} = \mathbf{C}^{-1}$ and $\mathbf{S}^0 = \mathbf{C}^{0^{-1}}$ are the elastic compliance of the original heterogeneous and background homogeneous solids, $\boldsymbol{\epsilon}^0$ is the eigenstrain field required for homogenization, and $\boldsymbol{\Lambda}$ is a linear operator producing from strain to a stress field with zero average. In other words,

$$\boldsymbol{\sigma}' = \boldsymbol{\Lambda}\boldsymbol{\epsilon}^0, \quad \langle\boldsymbol{\sigma}'\rangle = \mathbf{0}. \quad (19)$$

The explicit operation of $\boldsymbol{\Lambda}$ in the Fourier transform space can be obtained similarly by following the method proposed by Ref. 36 (see also the Appendix).

C. Total free energy

The total free energy of a martensite taking heterogeneous elastic moduli and microstructure into account is

$$\mathcal{I}^{tot} = \int \{W^{int} + W^{ani} + W^{elas}_{HS}\} d\mathbf{x}, \tag{20}$$

where the elastic energy density W^{elas} is replaced by W^{elas}_{HS} due to the result of Eq. (17). The first term in Eq. (20) is the *interfacial energy density* accounting for the surface energy of the interfaces between different variants of martensite, and the second term in Eq. (20) is the *anisotropy energy density* which is the energetic cost when field variables deviate from points corresponding to the ground states of energy wells. The explicit expressions of these two terms depend on the choices of phase filed variables. One newly approach, called an unconventional phase field model,[35–37] is to choose the characteristic functions of transforming variants as the field variables. For example, from Eq. (3), the characteristic function λ_i is used to represent each variant. Thus, W^{int} and W^{ani} can be expressed by[61]

$$W^{int} = A\sum_{i=1}^{N} |\nabla \lambda_i|^2, \tag{21}$$

$$W^{ani} = K_1\left[\sum_{i=1}^{N} \lambda_i^2 (1-\lambda_i)^2\right] + K_2\left[\sum_{i=1}^{N} \lambda_i - 1\right]^2, \tag{22}$$

where $A > 0$ is associated with the width of two adjacent martensitic variants and $K_1 > 0$ is related to the energy barrier from one energy ground state to the other. Note that the second term in W^{ani} with $K_2 > 0$ is required to avoid two variants occupying at the same material point.[61] This term can be removed by employing another characteristic function μ_i motivated by laminated microstructure such that

$$\begin{aligned} &\lambda_1 = \mu_1, \\ &\cdots \\ &\lambda_{N-1} = \mu_{N-1}(1-\mu_1)\cdots(1-\mu_{N-2}), \\ &\lambda_N = (1-\mu_1)\cdots(1-\mu_{N-2})(1-\mu_{N-1}). \end{aligned} \tag{23}$$

As a result, the anisotropy energy density can be expressed in terms of μ_i by $W^{ani} = K[\sum_{i=1}^{N} \mu_i^2(1-\mu_i)^2]$ with $K > 0$. Readers are referred to references for details of this approach.[35,37,62]

Taking the variations with respect to $\mathbf{p}$ and $\boldsymbol{\epsilon}^*$ in the total free energy, Eq. (20) gives

$$\delta\mathcal{I}^{tot} = -\int\left\{\mathbf{F}^{elas}_p \cdot \delta\mathbf{p} + \left(\mathbf{F}^{int} + \mathbf{F}^{ani} + \mathbf{F}^{elas}_{\varepsilon^*} \cdot \frac{\partial \boldsymbol{\epsilon}^*}{\partial \boldsymbol{\lambda}}\right) \cdot \delta\boldsymbol{\lambda}\right\} d\mathbf{x}, \tag{24}$$

where $\boldsymbol{\lambda} = (\lambda_1, \ldots, \lambda_N)$ and the driving forces $\mathbf{F}^{elas}_p$ and $\mathbf{F}^{elas}_{\varepsilon^*}$ are given by Eqs. (10) and (11), and the rest of two terms are

$$\mathbf{F}^{int} = 2A\nabla^2\boldsymbol{\lambda}, \quad \mathbf{F}^{ani} = -\frac{\partial W^{ani}}{\partial \boldsymbol{\lambda}}. \tag{25}$$

Physically, $\mathbf{F}^{int}$ is the driving force for coarsening microstructure and $\mathbf{F}^{ani}$ is the driving force for selecting variants. Note that periodic boundary conditions are enforced in deriving Eq. (24). But for non-periodic boundary conditions, the vanishing of normal derivative $\frac{\partial \boldsymbol{\lambda}}{\partial n} = \mathbf{0}$ is required on the boundary.[36]

D. Evolution equations

The thermodynamic driving forces are defined as the negative of the first variations with respect to fields variables $\mathbf{p}$ and $\boldsymbol{\lambda}$ in Eq. (20). It follows from Eq. (24) as

$$\begin{aligned} \mathbf{F}^p &= -\frac{\delta\mathcal{I}^{tot}}{\delta\mathbf{p}} = \mathbf{F}^{elas}_p, \\ \mathbf{F}^\lambda &= -\frac{\delta\mathcal{I}^{tot}}{\delta\boldsymbol{\lambda}} = \mathbf{F}^{int} + \mathbf{F}^{ansi} + \mathbf{F}^{elas}_{\varepsilon^*} \cdot \frac{\partial \boldsymbol{\epsilon}^*}{\partial \boldsymbol{\lambda}}. \end{aligned} \tag{26}$$

The evolution of polarized stress fields and martensitic variants is therefore assumed to be proportional to the associated thermodynamic driving forces; i.e.,

$$\begin{aligned} \frac{\partial \mathbf{p}}{\partial t} &= L^p \mathbf{F}^p \\ &= L^p\{-(\mathbf{C}^0 - \mathbf{C})^{-1}(\mathbf{p} - \mathbf{C}^0\boldsymbol{\epsilon}^*) + \boldsymbol{\Gamma}\mathbf{p} - \boldsymbol{\epsilon}^* + \langle\boldsymbol{\epsilon}\rangle\}, \end{aligned} \tag{27}$$

$$\begin{aligned} \frac{\partial \boldsymbol{\lambda}}{\partial t} &= L^\lambda \mathbf{F}^\lambda \\ &= L^\lambda\left\{2A\nabla^2\boldsymbol{\lambda} - \frac{\partial W^{ani}}{\partial \boldsymbol{\lambda}} + [\mathbf{C}^0(\mathbf{C}^0 - \mathbf{C})^{-1}(\mathbf{p} - \mathbf{C}^0\boldsymbol{\epsilon}^*) \right. \\ &\quad \left. -\mathbf{p} + \mathbf{C}^0\boldsymbol{\epsilon}^*] \cdot \frac{\partial \boldsymbol{\epsilon}^*}{\partial \boldsymbol{\lambda}}\right\}, \end{aligned} \tag{28}$$

where $L^p > 0$ and $L^\lambda > 0$ are the mobility coefficients. The evolution equations are interpreted as follows. When the driving force $\mathbf{F}^p$ is approaching to vanish under evolving from Eq. (27), this reaches the condition of Eq. (13) where the stress and strain fields in an equivalent homogeneous medium are identical to those in the original inhomogeneous solid. The final term $\mathbf{F}^{elas}_{\varepsilon^*}$ in Eq. (28) therefore corresponds to the actual stress driving evolution of microstructure, as interpreted by Eq. (14).

The total energy is decreased under the evolution of field variables. Indeed, from Eqs. (24), (27), and (28),

$$\begin{aligned} \frac{d\mathcal{I}^{tot}}{dt} &= -\int\left\{\mathbf{F}^{elas}_p \cdot \frac{\partial \mathbf{p}}{\partial t} + \left(\mathbf{F}^{int} + \mathbf{F}^{ani} + \mathbf{F}^{elas}_{\varepsilon^*} \cdot \frac{\partial \boldsymbol{\epsilon}^*}{\partial \boldsymbol{\lambda}}\right) \cdot \frac{\partial \boldsymbol{\lambda}}{\partial t}\right\} d\mathbf{x} \\ &= -\int L^p|\mathbf{F}^p|^2 d\mathbf{x} - \int L^\lambda|\mathbf{F}^\lambda|^2 d\mathbf{x} \le 0. \end{aligned} \tag{29}$$

Note that the mobility coefficient L^p in Eq. (27) could be replaced by $\tilde{L}^p(\mathbf{C}^0 - \mathbf{C})$ whenever $\tilde{L}^p > 0$ and $(\mathbf{C}^0 - \mathbf{C})$ is positive definite symmetric. The decrease of the total energy in Eq. (29) remains unchanged since $\tilde{L}^p(\mathbf{F}^p \cdot (\mathbf{C}^0 - \mathbf{C})\mathbf{F}^p) > 0$. Such a modification has been shown to be capable of enhancing the rate of convergence to an order of magnitude.[44]

Finally, if the boundary condition is replaced by assigning the average stress $\langle\boldsymbol{\sigma}\rangle$, the evolution equations become

$$\begin{aligned} \frac{\partial \boldsymbol{\epsilon}^0}{\partial t} &= -L^{\varepsilon^0}\frac{\delta\mathcal{I}^{tot}_*}{\delta\boldsymbol{\epsilon}^0} \\ &= L^{\varepsilon^0}\{-(\mathbf{S} - \mathbf{S}^0)^{-1}(\boldsymbol{\epsilon}^0 - \boldsymbol{\epsilon}^*) + \boldsymbol{\Lambda}\boldsymbol{\epsilon}^0 + \langle\boldsymbol{\sigma}\rangle\}, \end{aligned} \tag{30}$$

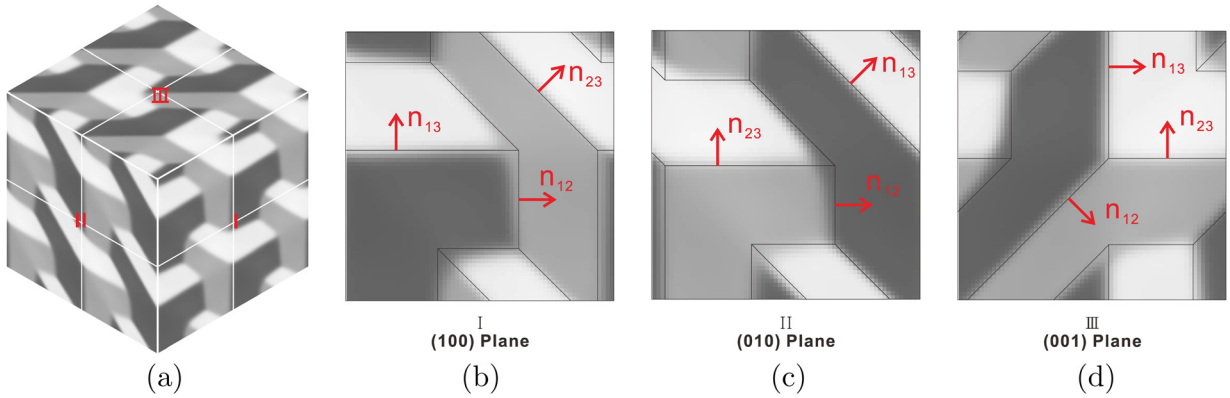

FIG. 2. A three-dimensional compatible self-accommodation pattern consisting of three tetragonal variants. The first variant is presented by the darkest gray level and the rest follows. (a) Eight identical patterns are packed together for exhibiting periodic images, (b) pattern projected to (100) plane, (c) pattern projected to (010) plane, and (d) pattern projected to (001) plane.

$$\frac{\partial \boldsymbol{\lambda}}{\partial t} = -L^{\lambda}\frac{\delta \mathcal{I}_*^{tot}}{\delta \boldsymbol{\lambda}} = L^{\lambda}\left\{2A\nabla^2\boldsymbol{\lambda} - \frac{\partial W^{ani}}{\partial \boldsymbol{\lambda}} + [(\mathbf{S}-\mathbf{S}^0)^{-1}(\boldsymbol{\epsilon}^0-\boldsymbol{\epsilon}^*)]\cdot\frac{\partial \boldsymbol{\epsilon}^*}{\partial \boldsymbol{\lambda}}\right\}, \tag{31}$$

where mobility coefficients $L^{\varepsilon^0} > 0, L^{\lambda} > 0$, and $\mathcal{I}_*^{tot}$ replace the third term of $\mathcal{I}^{tot}$ by W_{HS*}^{elas}; i.e.,

$$\mathcal{I}_*^{tot} = \int\{W^{int} + W^{ani} + W_{HS*}^{elas}\}d\mathbf{x},$$

and W_{HS*}^{elas} is defined by Eq. (18).

III. RESULTS

Consider the case of tetragonal martensite first. The parameters of transformation strain are taken to be $\eta_1 = -1.5\%$ and $\eta_2 = 3\%$ in Eq. (1). As the elastic properties of single crystals are not available for typical shape-memory alloys, the data from $PbTiO_3$ ferroelectric crystals in the tetragonal phase are chosen instead.[63] For the first variant, they are $C_{11}^{(1)} = 235$ GPa, $C_{33}^{(1)} = 105$ GPa, $C_{12}^{(1)} = 101$ GPa, $C_{13}^{(1)} = 98.8$ GPa, $C_{44}^{(1)} = 65.1$ GPa, and $C_{66}^{(1)} = 104$ GPa where the Voigt notation is adopted here. The elastic modulus for other variants can be obtained by symmetry transformation. In addition, the elastic modulus of the comparison material is chosen to be $\frac{2}{3}(\mathbf{C}^{(1)} + \mathbf{C}^{(2)} + \mathbf{C}^{(3)})$ to guarantee that $(\mathbf{C}^0 - \mathbf{C}^{(i)})$ is positive definite for $i = 1, 2, 3$. The evolution equations in Eqs. (27) and (28) are numerically computed in a unit cell with $K_1 = K_2 = 0.557$ GPa and $A = 0.0001K_1$. To enhance the rate of convergence, the Fast Fourier Transform (FFT) is carried out for evaluating the operation $\boldsymbol{\Gamma}$ in Eq. (8). The random initial conditions are taken for simulations.

Self-accommodation patterns are of the primary interest in shape-memory alloys,[64] and therefore, the average strain is assigned by $\langle\boldsymbol{\epsilon}\rangle = \mathbf{0}$. A 3-dimensional simulation result is shown in Fig. 2(a), where different martensitic variants are presented by different gray levels. The darkest shadow denotes the first variant and the rest follows. Notice that the microstructure patterns projected to (100)/(010)/(001) planes are marked as I, II, and III in Fig. 2(a). Each of them is also presented in Figs. 2(b)–2(d), respectively. While the gray levels become a little blurred at the triple junctions in each plot, the rest shows sufficient resolution for distinguishing different martensitic variants. Several comments are made below.

First, the pattern shown in Fig. 2(a) is not a typical rank-2 laminate where two fine-scale lamellar microstructure patterns alternate in layers separated by parallel planes (for example, see the pattern comprised by trigonal variants in Fig. 3). Instead, it is an intriguing, fascinating, and strain-

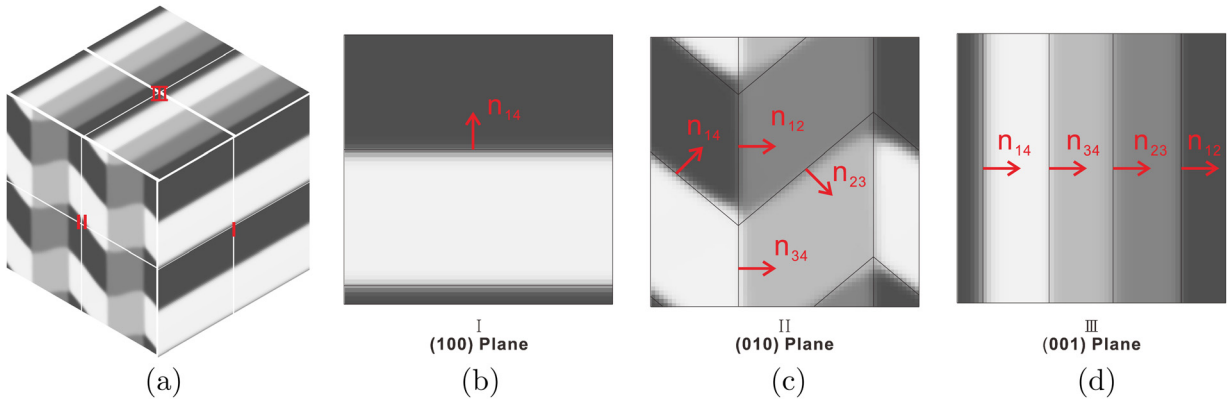

FIG. 3. A three-dimensional compatible self-accommodation pattern consisting of four trigonal variants. The first variant is presented by the darkest gray level and the rest follows. (a) Eight identical patterns are packed together for exhibiting periodic images, (b) pattern projected to (100) plane, (c) pattern projected to (010) plane, and (d) pattern projected to (001) plane.

TABLE I. Three-dimensional compatible interfaces formed by different pairs of tetragonal variants are listed. The interfacial normals projected onto different cubic faces are also listed.

	Tetragonal martensite		
	$\epsilon_{tet}^{(1)}/\epsilon_{tet}^{(2)}$	$\epsilon_{tet}^{(1)}/\epsilon_{tet}^{(3)}$	$\epsilon_{tet}^{(2)}/\epsilon_{tet}^{(3)}$
3D	$(110)/(1\bar{1}0)$	$(101)/(10\bar{1})$	$(011)/(01\bar{1})$
(100) plane	$(1\,0)$	$(0\,1)$	$(1\,1)/(1\,\bar{1})$
(010) plane	$(1\,0)$	$(1\,1)/(1\,\bar{1})$	$(0\,1)$
(001) plane	$(1\,1)/(1\,\bar{1})$	$(1\,0)$	$(0\,1)$

compatible pattern. Indeed, two variants i and j are twin-related (or compatible) if they satisfy

$$\boldsymbol{\epsilon}^{(i)} - \boldsymbol{\epsilon}^{(j)} = \frac{1}{2}(\mathbf{a} \otimes \mathbf{n} + \mathbf{n} \otimes \mathbf{a}) \tag{32}$$

for some vectors $\mathbf{a}$ and $\mathbf{n}$.[1] If such a relation holds, they can form a lamellar microstructure with interfacial normal parallel to $\mathbf{n}$. Table I lists all possible 3-dimensional compatible interfaces formed by different pairs of tetragonal variants. In addition, the interfacial normals projected to (100), (010), and (001) planes are also listed in Table I. For example, consider the (100) face which is marked the symbol I in Fig. 2(a) and is also shown in Fig. 2(b). It is found that the interfaces between the first and second variants and the interfaces between the first and third variants are parallel to the edges (see $\mathbf{n}_{12}$ and $\mathbf{n}_{13}$). Further, the interfaces between the second and the third variants are $45^\circ(135^\circ)$ oriented from the edges (see $\mathbf{n}_{23}$). These observations agree well with those listed in Table I. Similarly, the patterns projected to (010) and (001) planes shown in Figs. 2(c) and 2(d) also follow the rules of compatibility listed in Table I.

Next, consider the case of trigonal martensite. The parameters of transformation strain are taken to be $\alpha = 0$ and $\delta = 0.1\%$ in Eq. (2). Similar to the explanation in previous case, the elastic constants are chosen from the data of $Pb(Zn_{1/3}Nb_{2/3})O_3 - PbTiO_3$ (PZN-PT) ferroelectric crystals in the trigonal phase.[65] They are for the first variant $C_{11}^{(1)} = 180\,\text{GPa}$, $C_{12}^{(1)} = 80\,\text{GPa}$, $C_{13}^{(1)} = 48\,\text{GPa}$, $C_{14}^{(1)} = -26$ GPa, $C_{33}^{(1)} = 171\,\text{GPa}$, and $C_{44}^{(1)} = 16\,\text{GPa}$ where the data are measured based on the crystal basis of the trigonal phase. The elastic modulus of the comparison material is chosen to be $\frac{5}{4}(\mathbf{C}^{(1)} + \mathbf{C}^{(2)} + \mathbf{C}^{(3)} + \mathbf{C}^{(4)})$ to guarantee that $(\mathbf{C}^0 - \mathbf{C}^{(i)})$ is positive definite for $i = 1, \ldots, 4$. The evolution equations in Eqs. (27) and (28) are numerically computed in a unit cell with $K_1 = K_2 = 1.93\,\text{MPa}$ and $A = 0.0001K_1$.

The average strain is assigned by $\langle \boldsymbol{\epsilon} \rangle = \mathbf{0}$ for producing self-accommodation patterns. A three-dimensional simulation result is shown in Fig. 3(a), where different martensitic variants are presented by different gray levels. The darkest shadow denotes the first variant and the rest follows. Notice that the microstructure patterns projected to (100)/(010)/(001) planes are marked as I, II, and III in Fig. 3(a). Each of them is also presented in Figs. 3(b)–3(d). Similar to the previous case, there is a little blurred in gray levels at the triple junctions. But the rest of regions shows clear resolution for identifying distinct martensitic variants. Next, in contrast to the previous case, the pattern shown in Fig. 3(a) is a typical rank-2 laminate. It exhibits a standard compatible herringbonelike structure.[29,37] To see it, first note that Table II lists all possible three-dimensional compatible interfaces satisfying Eq. (32) for different pairs of trigonal variants. In addition, there are two types of twins classified by their interfacial normals. One is the {100} type-I twin and the other is the {110} type-II twin. The interfacial normals projected to (100), (010), and (001) planes are also listed in Table II. The subscripts of the projected normals indicate what types of twins they originally come from. To examine the issue of strain compatibility, take an example of the (010) face which is marked the symbol II in Fig. 3(a) and is also shown in Fig. 3(c). Four trigonal variants are arranged to form a compatible herringbone structure. Indeed, from Table II, the only compatible interface between the first and fourth variants is the one with normal $(11)_2$ projected to the (010) plane, and the subscript 2 indicates the type-II twin originally. In addition, the only compatible interface between the second and third variants is the one with normal $(1\bar{1})_2$ projected to the (010) plane. These predictions are observed in Fig. 3(c) by the labels indicating normals $\mathbf{n}_{14}$ and $\mathbf{n}_{23}$, respectively. Similarly, the projected normals $\mathbf{n}_{12}$ and $\mathbf{n}_{34}$ in Fig. 3(c) are along the (10) direction. Both agree well with those predicted in Table II. Finally, the examination of interfaces shown in Figs. 3(b) and 3(d) confirms that they do follow exactly the rules of compatibility listed in Table II.

IV. CONCLUSIONS

An unconventional phase-field model taken into account elastic modulus difference of distinct phases is established for microstructure simulation in martensitic materials. It is based on the Hashin-Shtrikman variational formulation by introducing a homogeneous comparison elastic material and a polarized stress field so that strain and stress fields in an

TABLE II. Three-dimensional compatible interfaces formed by different pairs of trigonal variants are listed. The interfacial normals projected onto different cubic faces are also listed.

	Trigonal martensite					
	$\epsilon_{trig}^{(1)}/\epsilon_{trig}^{(2)}$	$\epsilon_{trig}^{(1)}/\epsilon_{trig}^{(3)}$	$\epsilon_{trig}^{(1)}/\epsilon_{trig}^{(4)}$	$\epsilon_{trig}^{(2)}/\epsilon_{trig}^{(3)}$	$\epsilon_{trig}^{(2)}/\epsilon_{trig}^{(4)}$	$\epsilon_{trig}^{(3)}/\epsilon_{trig}^{(4)}$
3D	(100)/(011)	(001)/(110)	(010)/(101)	$(010)/(10\bar{1})$	$(001)/(1\bar{1}0)$	$(100)/(01\bar{1})$
(100) plane	$(1\,1)_2$	$(0\,1)_1/(1\,0)_2$	$(1\,0)_1/(0\,1)_2$	$(1\,0)_1/(0\,1)_2$	$(0\,1)_1/(1\,0)_2$	$(1\,\bar{1})_2$
(010) plane	$(1\,0)_1/(0\,1)_2$	$(0\,1)_1/(1\,0)_2$	$(1\,1)_2$	$(1\,\bar{1})_2$	$(0\,1)_1/(1\,0)_2$	$(1\,0)_1/(0\,1)_2$
(001) plane	$(1\,0)_1/(0\,1)_2$	$(1\,1)_2$	$(0\,1)_1/(1\,0)_2$	$(0\,1)_1/(1\,0)_2$	$(1\,\bar{1})_2$	$(1\,0)_1/(0\,1)_2$

equivalent homogeneous medium are identical to those in the original inhomogeneous solid. As a result, the force due to stress for driving microstructure evolution is able to be computed in the homogeneous comparison solid to which the fast numerical algorithm can be applied. The framework is applied to the simulation of three-dimensional self-accommodation patterns for tetragonal and trigonal martensitic materials. The former produces an atypical but fascinating and compatible pattern, while the latter is a commonly observed herringbone structure. Finally, as the unconventional phase field models have shown easiness in coupling multiple physical processes and order parameters,[66–68] the proposed framework extended to other phase-transforming materials accounting for material inhomogeneities is currently under investigation.[58]

ACKNOWLEDGMENTS

The authors are glad to acknowledge the financial support of the National Science Council of Taiwan under the Grant No. NSC 100-2628-E-002-034-MY3, and the partial support from the Career Development Project of National Taiwan University.

APPENDIX: FOURIER TRANSFORM OF STRESS FIELD IN A STRUCTURALLY INHOMOGENEOUS BUT ELASTIC HOMOGENEOUS SOLID

Let $\bar{f}(\boldsymbol{\xi})$ be the Fourier transform of any function $f(\mathbf{x})$, where $\mathbf{x} = (x_1, x_2, x_3)$ and $\boldsymbol{\xi} = (\xi_1, \xi_2, \xi_3)$ are the coordinates in the real and reciprocal spaces. Both $f(\mathbf{x})$ and $\bar{f}(\boldsymbol{\xi})$ are related by

$$\bar{f}(\boldsymbol{\xi}) = \mathcal{F}[f] = \int_{-\infty}^{\infty} f(\mathbf{x}) e^{-2\pi i(\boldsymbol{\xi}\cdot\mathbf{x})} d\mathbf{x}, \tag{A1}$$

$$f(\mathbf{x}) = \mathcal{F}^{-1}[\bar{f}] = \int_{-\infty}^{\infty} \bar{f}(\boldsymbol{\xi}) e^{2\pi i(\boldsymbol{\xi}\cdot\mathbf{x})} d\boldsymbol{\xi}, \tag{A2}$$

where $i^2 = -1$.

Let $\mathbf{p}$ denote the polarized stress with $\bar{\mathbf{p}}$ as its Fourier transform. It produces a strain $\boldsymbol{\epsilon}$ with $\bar{\boldsymbol{\epsilon}}$ as its Fourier transform. Suppose both are expressed in terms of Voigt notation. Thus, it can be shown that they are related by $\bar{\boldsymbol{\epsilon}} = \hat{\boldsymbol{\Gamma}}\bar{\mathbf{p}}$ in the Fourier transform space[36] with

$$\hat{\boldsymbol{\Gamma}} = \mathbf{B}(\mathbf{B}^T\mathbf{C}^0\mathbf{B})^{-1}\mathbf{B}^T. \tag{A3}$$

Above, $\mathbf{C}^0$ is the elastic 4-tensor of a homogeneous comparison material expressed in terms of Voigt notation, and

$$\mathbf{B} = 2\pi i \begin{pmatrix} \xi_1 & 0 & 0 \\ 0 & \xi_2 & 0 \\ 0 & 0 & \xi_3 \\ 0 & \xi_3 & \xi_2 \\ \xi_3 & 0 & \xi_1 \\ \xi_2 & \xi_1 & 0 \end{pmatrix}.$$

Next, let $\boldsymbol{\epsilon}^0$ denote the eigenstrain field necessary for homogenization and let $\bar{\boldsymbol{\epsilon}}^0$ be its Fourier transform. It produces a stress $\boldsymbol{\sigma}$ with $\bar{\boldsymbol{\sigma}}$ as its Fourier transform. It can be shown similarly that both are related by $\bar{\boldsymbol{\sigma}} = \hat{\boldsymbol{\Lambda}}\bar{\boldsymbol{\epsilon}}^0$ in the Fourier transform space[36] with

$$\hat{\boldsymbol{\Lambda}} = \mathbf{C}^0[\mathbf{B}(\mathbf{B}^T\mathbf{C}^0\mathbf{B})^{-1}\mathbf{B}^T\mathbf{C}^0 - \mathbf{I}], \tag{A4}$$

where $\mathbf{I}$ is the identity.

[1] K. Bhattacharya, *Microstructure of Martensite* (Oxford University Press, Oxford, 2003).
[2] *Shape Memory Alloys: Modeling and Engineering Applications*, edited by D. C. Lagoudas (Springer, 2008).
[3] S. Miyazaki, S. Kimura, and K. Otsuka, "Shape-memory effect and pseudoelasticity associated with the R-phase transition in Ti-50.5 at. % Ni single crystals," Philos. Mag. A **57**, 467–478 (1988).
[4] K. Bhattacharya and R. D. James, "The material is the machine," Science **307**, 53–54 (2005).
[5] D. C. Lagoudas, P. B. Entchev, P. Popov, E. Patoor, L. C. Brinson, and X. J. Gao, "Shape memory alloys, Part II: Modeling of polycrystals," Mech. Mater. **38**, 430–462 (2006).
[6] V. I. Levitas, A. V. Idesman, and D. L. Preston, "Microscale simulation of martensitic microstructure evolution," Phys. Rev. Lett. **93**, 105701 (2004).
[7] Z. K. Lu and G. J. Weng, "Martensitic transformation and stress-strain relations of shape-memory alloys," J. Mech. Phys. Solids **45**, 1905–1928 (1997).
[8] Q. P. Sun, K. C. Hwang, and S. W. Yu, "A micromechanics constitutive model of transformation plasticity with shear and dilatation effect," J. Mech. Phys. Solids **39**, 507–524 (1991).
[9] J. S. Bowles and J. K. MacKenzie, "The crystallography of martensite transformations I and II," Acta Metall. **2**, 129–137 and 138–147 (1954).
[10] M. Wechsler, D. Lieberman, and T. Read, "On the theory of the formation of martensite," Trans. AIME **197**, 1503–1515 (1953).
[11] J. M. Ball and R. D. James, "Fine phase mixtures as minimizers of energy," Arch. Ration. Mech. Anal. **100**, 13–52 (1987).
[12] A. G. Khachaturyan, *Theory of Structural Transformations in Solids* (Wiley, New York, 1983).
[13] A. L. Roitburd, "Martensitic transformation as a typical phase transformation in solids," Solid State Phys. **33**, 317–390 (1978).
[14] J. Deng, X. Ding, T. Lookman, T. Suzuki, K. Otsuka, J. Sun, A. Saxena, and X. Ren, "Microscopic mechanism of martensitic stabilization in shape-memory alloys: Atomic-level processes," Phys. Rev. B **81**, 220101(R) (2010).
[15] O. Kastner, G. Eggeler, W. Weiss, and G. J. Ackland, "Molecular dynamics simulation study of microstructure evolution during cyclic martensitic transformations," J. Mech. Phys. Solids **59**, 1888–1908 (2011).
[16] C. T. Lu and K. Dayal, "Linear instability signals the initiation of motion of a twin plane under load," Philos. Mag. Lett. **91**, 264–271 (2011).
[17] N. T. Tsou and J. E. Huber, "Compatible domain structures and the poling of single crystal ferroelectrics," Mech. Mater. **42**, 740–753 (2010).
[18] N. T. Tsou, J. E. Huber, and Y. C. Shu, "A sharp interface model of compatible twin patterns in shape memory alloys," Smart Mater. Struct. **21**, 094010 (2012).
[19] F. X. Li, X. L. Zhou, and A. K. Soh, "An optimization-based "phase field" model for polycrystalline ferroelectrics," Appl. Phys. Lett. **96**, 152905 (2010).
[20] Y. Su and C. M. Landis, "Continuum thermodynamics of ferroelectric domain evolution: Theory, finite element implementation, and application to domain wall pinning," J. Mech. Phys. Solids **55**, 280–305 (2007).
[21] B. Volker, C. M. Landis, and M. Kamlah, "Multiscale modeling for ferroelectric materials: identification of the phase-field model's free energy for PZT from atomistic simulations," Smart Mater. Struct. **21**, 035025 (2012).
[22] Y. F. Xia and J. Wang, "Switching behavior of ferroelectric thin films with deadlayers," Smart Mater. Struct. **21**, 094019 (2012).
[23] L. Yang and K. Dayal, "Real-space phase-field simulation of piezoresponse force microscopy accounting for stray electric fields," Modell. Simul. Mater. Sci. Eng. **20**, 035021 (2012).
[24] A. Artemev, Y. Jin, and A. G. Khachaturyan, "Three-dimensional phase field model of proper martensitic transformation," Acta Mater. **49**, 1165–1177 (2001).
[25] Y. Wang and A. G. Khachaturyan, "Three-dimensional field model and computer modeling of martensitic transformations," Acta Mater. **45**, 759–773 (1997).

[26]A. Artemev, Y. Wang, and A. G. Khachaturyan, "Three-dimensional phase field model and simulation of martensitic transformation in multilayer systems under applied stresses," Acta Mater. **48**, 2503–2518 (2000).
[27]J. Slutsker, A. Artemev, and A. L. Roytburd, "Engineering of elastic domain structures in a constrained layer," Acta Mater. **52**, 1731–1742 (2004).
[28]A. Artemev, Y. Jin, and A. G. Khachaturyan, "Three-dimensional phase field model and simulation of cubic → Tetragonal martensitic transformation in polycrystals," Philos. Mag. A **82**, 1249–1270 (2002).
[29]Y. M. Jin, A. Artemev, and A. G. Khachaturyan, "Three-dimensional phase field model of low-symmetry martensitic transformation in polycrystal: Simulation of ζ_2' martensite in AuCd alloys," Acta Mater. **49**, 2309–2320 (2001).
[30]R. Ahluwalia, T. Lookman, A. Saxena, and R. C. Albers, "Landau theory for shape memory polycrystals," Acta Mater. **52**, 209–218 (2004).
[31]A. E. Jacobs, S. H. Curnoe, and R. C. Desai, "Simulations of cubic-tetragonal ferroelastics," Phys. Rev. B **68**, 224104 (2003).
[32]T. Lookman, S. R. Shenoy, K. Ø. Rasmussen, A. Saxena, and A. R. Bishop, "Ferroelastic dynamics and strain compatibility," Phys. Rev. B **67**, 024114 (2003).
[33]L. Q. Chen, "Phase-field models for microstructure evolution," Annu. Rev. Mater. Res. **32**, 113–140 (2002).
[34]J. Y. Li, C. H. Lei, L. J. Li, Y. C. Shu, and Y. Y. Liu, "Unconventional phase field simulations of transforming materials with evolving microstructures," Acta Mech. Sin. **28**, 915–927 (2012).
[35]Y. C. Shu and J. H. Yen, "Pattern formation in martensitic thin films," Appl. Phys. Lett. **91**, 021908 (2007).
[36]Y. C. Shu and J. H. Yen, "Multivariant model of martensitic microstructure in thin films," Acta Mater. **56**, 3969–3981 (2008).
[37]Y. C. Shu, J. H. Yen, H. Z. Chen, J. Y. Li, and L. J. Li, "Constrained modeling of domain patterns in rhombohedral ferroelectrics," Appl. Phys. Lett. **92**, 052909 (2008).
[38]J. D. Eshelby, "The determination of the elastic field of an ellipsoidal inclusion, and related problems," Proc. R. Soc. London, Ser. A **241**, 376–396 (1957).
[39]Y. U. Wang, Y. M. Jin, and A. G. Khachaturyan, "Phase field microelasticity theory and modeling of elastically and structurally inhomogeneous solid," J. Appl. Phys. **92**, 1351–1360 (2002).
[40]L. Lei, J. L. Marin, and M. Koslowski, "Phase-field modeling of defect nucleation and propagation in domains with material inhomogeneities," Modell. Simul. Mater. Sci. Eng. **21**, 025009 (2013).
[41]Y. Ni and M. Y. M. Chiang, "Prediction of elastic properties of heterogeneous materials with complex microstructures," J. Mech. Phys. Solids **55**, 517–532 (2007).
[42]Y. Ni, L. He, and A. G. Khachaturyan, "Equivalency principle for magnetoelectroelastic multiferroics with arbitrary microstructure: The phase field approach," J. Appl. Phys. **108**, 023504 (2010).
[43]Y. Ni and L. H. He, "Spontaneous formation of vertically anticorrelated epitaxial islands on ultrathin substrates," Appl. Phys. Lett. **97**, 261911 (2010).
[44]Y. Shen, Y. Li, Z. Li, H. Wan, and P. Nie, "An improvement on the three-dimensional phase-field microelasticity theory for elastically and structurally inhomogeneous solids," Scr. Mater. **60**, 901–904 (2009).
[45]J. J. Wang, S. Bhattacharyya, Q. Li, T. W. Heo, X. Q. Ma, and L. Q. Chen, "Elastic solutions with arbitrary elastic inhomogeneity and anisotropy," Philos. Mag. Lett. **92**, 327–335 (2012).
[46]S. Bhattacharyya, K. Chang T. W. Heo, and L. Q. Chen, "A phase-field model of stress effect on grain boundary migration," Modell. Simul. Mater. Sci. Eng. **19**, 035002 (2011).
[47]S. Y. Hu and L. Q. Chen, "A phase-field model for evolving microstructures with strong elastic inhomogeneity," Acta Mater. **49**, 1879–1890 (2001).
[48]H. Moulinec and P. Suquet, "A fast numerical method for computing the linear and nonlinear mechanical properties of composites," C. R. Seances Acad. Sci., Ser. 2 **318**, 1417–1423 (1994).
[49]H. Moulinec and P. Suquet, "A numerical method for computing the overall response of nonlinear composites with complex microstructure," Comput. Methods Appl. Mech. Eng. **157**, 69–94 (1998).
[50]H. Moulinec and P. Suquet, "Comparison of FFT-based methods for computing the response of composites with highly contrasted mechanical properties," Physica B **338**, 58–60 (2003).
[51]J. C. Michel, H. Moulinec, and P. Suquet, "Effective properties of composite materials with periodic microstructure: A computational approach," Comput. Methods Appl. Mech. Eng. **172**, 109–143 (1999).
[52]J. C. Michel, H. Moulinec, and P. Suquet, "A computational method based on augmented Lagrangians and fast Fourier transforms for composites with high contrast," Comput. Model. Eng. Sci. **1**, 79–88 (2000).
[53]J. C. Michel, H. Moulinec, and P. Suquet, "A computational scheme for linear and non-linear composites with arbitrary phase contrast," Int. J. Numer. Methods Eng. **52**, 139–160 (2001).
[54]Z. Hashin and S. Shtrikman, "A variational approach to the theory of the elastic behaviour of multiphase materials," J. Mech. Phys. Solids **11**, 127–140 (1963).
[55]J. R. Willis, "Bounds and self-consistent estimates for the overall properties of anisotropic composites," J. Mech. Phys. Solids **25**, 185–202 (1977).
[56]J. Y. Li and D. Liu, "On ferroelectric crystals with engineered domain configurations," J. Mech. Phys. Solids **52**, 1719–1742 (2004).
[57]D. Liu and J. Y. Li, "The enhanced and optimal piezoelectric coefficients in single crystalline barium titanate with engineered domain configurations," Appl. Phys. Lett. **83**, 1193–1195 (2003).
[58]H. Z. Chen, Ph.D. dissertation, National Taiwan University (in preparation).
[59]Y. C. Shu and K. Bhattacharya, "The influence of texture on the shape-memory effect in polycrystals," Acta Mater. **46**, 5457–5473 (1998).
[60]K. Enami and S. Nenno, "Memory effect in Ni-36.8 at. pct. Al martensite," Metall. Trans. **2**, 1487–1490 (1971).
[61]L. Yang and K. Dayal, "Formulation of phase-field energies for microstructure in complex crystal structures," Appl. Phys. Lett. **96**, 081916 (2010).
[62]Y. C. Shu, J. H. Yen, J. Shieh, and J. H. Yeh, "Effect of depolarization and coercivity on actuation strains due to domain switching in barium titanate," Appl. Phys. Lett. **90**, 172902 (2007).
[63]Z. Li, M. Grimsditch, X. Xu, and S. K. Chan, "The elastic, piezoelectric and dielectric constants of tetragonal $PbTiO_3$ single crystals," Ferroelectrics **141**, 313–325 (1993).
[64]S. Miyazaki, K. Otsuka, and C. M. Wayman, "The shape memory mechanism associated with the martensitic transformation in Ti-Ni alloys—I. Self-accommodation," Acta Metall. **37**, 1873–1884 (1989).
[65]J. Jin, K. K. Rajan, and L. C. Lim, "Properties of single domain $Pb(Zn_{1/3}Nb_{2/3})O_3 - (6-7)\%PbTiO_3$ single crystal," Jpn. J. Appl. Phys., Part 1 **45**, 8744–8747 (2006).
[66]L. J. Li, C. H. Lei, Y. C. Shu, and J. Y. Li, "Phase-field simulation of magnetoelastic couplings in ferromagnetic shape memory alloys," Acta Mater. **59**, 2648–2655 (2011).
[67]L. J. Li, J. Y. Li, Y. C. Shu, and J. H. Yen, "The magnetoelectric domains and cross-field switching in multiferroic $BiFeO_3$," Appl. Phys. Lett. **93**, 192506 (2008).
[68]L. J. Li, Y. Yang, Y. C. Shu, and J. Y. Li, "Continuum theory and phase-field simulation of magnetoelectric effects in multiferroic bismuth ferrite," J. Mech. Phys. Solids **58**, 1613–1627 (2010).